

Resource Allocation via Model-Free Deep Learning in Free Space Optical Networks

Zhan Gao*, Mark Eisen†, and Alejandro Ribeiro*

Abstract—This paper investigates the general problem of resource allocation for mitigating channel fading effects in Free Space Optical (FSO) networks. The resource allocation problem is modelled with a constrained stochastic optimization framework, which we exemplify with problems in power adaptation and relay selection. Under this framework, we develop two algorithms to solve FSO resource allocation problems. We first present the Stochastic Dual Gradient algorithm that solves the problem exactly by exploiting the null duality gap but whose implementation necessarily requires explicit and accurate system models. As an alternative we present the Primal-Dual Deep Learning algorithm, which parametrizes the resource allocation policy with Deep Neural Networks (DNNs) and optimizes via a primal-dual method. The parametrized resource allocation problem incurs only a small loss of optimality due to the strong representational power of DNNs, and can be moreover implemented in an unsupervised manner without knowledge of system models. Numerical experiments are performed to exhibit superior performance of proposed algorithms compared to baseline methods in a variety of resource allocation problems in FSO networks, including both continuous power allocation and binary relay selection.

Index Terms—Free space optical networks, deep learning, power adaptation, relay selection

I. INTRODUCTION

Free Space Optical (FSO) communication has attracted noticeable attention in both academia and industry due to its high capacity, low cost, strong security and flexible construction [2]–[4]. FSO communication transmits signals with optical carriers through the atmosphere and has found wide applications in satellite communications [5], last-mile access [6], fiber backup [7] and fronthaul or backhaul for wireless cellular networks [8]. Despite this potential, FSO communication is susceptible to channel characteristics, i.e., its performance can be seriously degraded by factors such as weather conditions, atmospheric turbulence and background radiation [9]. Different models have been proposed to characterize the FSO channel, based on which a number of techniques are developed to mitigate channel effects [10]–[16]. Cooperative transmission has recently been introduced as one of such techniques in FSO networks, which improves the system performance by

leveraging optimal resource allocation [17]–[19]. Cooperative transmission allocates resources adaptively based on the channel state information (CSI) in order to optimize the system performance. Common examples of FSO resource allocation problems include power adaptation and relay selection.

Power adaptation has emerged as a popular cooperative transmission technique to mitigate channel fading effects. With total power and peak power constraints, adaptive powers are assigned to orthogonal wavelength channels to achieve the optimal channel capacity [20]–[22]. Relay-assisted communication, on the other hand, employs multiple relay nodes between the transmitter and the receiver to create a virtual multiple-aperture system [23]–[25]. It utilizes advantages of multiple-input multiple-output (MIMO) systems by building multiple independent FSO channels and facilitates communication by avoiding obstacle blocking in the line-of-sight link between the transmitter and the receiver. Parallel and serial (multihop) relaying configurations are proposed with amplify-and-forward and decode-and-forward relaying strategies. However, it is not practical to activate all available relays that requires perfect transmission synchronization. To address this issue, different relay selection algorithms are developed that only activate a single relay at each hop based on the CSI while achieving good performance [26], [27].

Joint power adaptation and relay selection algorithms have been further developed to maximize the network throughput and minimize the outage probability in FSO networks [28], [29]. However, the aforementioned works apply approximation approaches to simplify optimization problems resulting in inexact solutions and are usually of high computational complexity. Furthermore, these solutions depend on system models (e.g., capacity functions and channel distributions) which may be inaccurate in practice.

These challenges and shortcomings of existing FSO resource allocation methods make the application of machine learning methods appealing, due to their low complexity and potential for model-free implementations. Deep Neural Networks (DNNs) have been developed as predominant tools to analyze data for target information and have achieved resounding successes in many communication, signal processing and control problems [30]–[32]. In particular, DNNs have been applied for resource allocation problems in wireless radio frequency (RF) domain in both supervised [33] and unsupervised manners [34], [35]. While to the best of our knowledge, such approaches have not yet been explored in FSO systems.

In this paper we study the general resource allocation problem in FSO communication networks. We first formulate

The work in this paper was supported by ARL DCIST CRA W911NF-17-2-0181, NSF HDR TRIPADS 1934960, and the Intel Science and Technology Center in Wireless Autonomous Systems. Preliminary results appear in GLOBECOM 2019 conference [1]. *Department of Electrical and Systems Engineering, University of Pennsylvania, Philadelphia, PA (Email: {gaozhan,aribeiro}@seas.upenn.edu). †Intel Corporation, Hillsboro, OR (Email: mark.eisen@intel.com).

This work has been submitted to the IEEE for possible publication. Copyright may be transferred without notice, after which this version may no longer be accessible.

the resource allocation problem as the constrained stochastic optimization problem in which we seek an optimal resource allocation policy that adapts to the fading state of the network (Section II). As examples, we in particular consider problems of power adaptation in Radio over FSO systems (Section II-A), relay selection in relay-assisted FSO networks (Section II-B), and joint power and relay allocation in FSO fronthaul networks (Section II-C). Resource allocation problems of this form are typically challenging due to non-convex objectives, infinite dimensionality of the resource allocation policy, existence of constraints, and lack of model knowledge.

We address each of these issues through the use of Lagrangian duality and model-free learning. We first propose the Stochastic Dual Gradient (SDG) algorithm that solves the problem exactly by utilizing the idea of strong duality in [36] (Section III). Strong duality permits us to operate in the dual domain, which is convex, unconstrained, and finite dimensional. Despite the theoretical advantages, this algorithm is limited in practice as it is dependent upon system models and requires expensive computations to implement. As a model-free and low complexity alternative, we leverage machine learning techniques to develop the Primal-Dual Deep Learning (PDDL) algorithm (Section IV). In particular, DNNs are employed to parameterize the resource allocation policy, which are trained with an unsupervised primal-dual method to solve the constrained learning problem. A model-free implementation is obtained by using the policy gradient method, which is particularly useful when FSO system and channel models are inaccurate or unknown. Numerical experiments are performed in four applications, involving both power adaptation and relay selection, to illustrate the benefits of the proposed algorithms against baseline methods (Section V).

II. PROBLEM FORMULATION

Consider a general free space optical (FSO) communication system under some form of resource constraints. By adaptively allocating resources using a policy that responds to instantaneous fading effects of the atmospheric channel, we can mitigate these fading effects and optimize the system performance. Denote by $\mathbf{h} \in \mathbb{R}^m$ the collected channel state information (CSI) of the FSO system and $\mathbf{r}(\mathbf{h}) \in \mathbb{R}^n$ a policy that determines the allocated resources based on the observed \mathbf{h} . The objective function $f(\mathbf{h}, \mathbf{r}(\mathbf{h}))$ measures the system performance that is instantiated on \mathbf{h} and $\mathbf{r}(\mathbf{h})$. Furthermore, a total of S constraints are imposed either on the resources $\mathbf{r}(\mathbf{h})$ or on the objective function $f(\mathbf{h}, \mathbf{r}(\mathbf{h}))$, each of which represented by a constraint function $c_s(\mathbf{r}(\mathbf{h}), f(\mathbf{h}, \mathbf{r}(\mathbf{h})))$ for all $s = 1, \dots, S$. The atmospheric channel is typically considered as a fading process with channel coherence time on the order of milliseconds, such that we shall assume \mathbf{h} is drawn from an ergodic and i.i.d block fading process. In this case, the instantaneous system performance tends to vary fast and the long term average performance $\mathbb{E}_{\mathbf{h}}[f(\mathbf{h}, \mathbf{r}(\mathbf{h}))]$ is the more meaningful metric to consider when designing an optimal resource allocation policy. We similarly consider constraints to be satisfied in expectation as well.

Our goal is then to maximize the expected performance $\mathbb{E}_{\mathbf{h}}[f(\mathbf{h}, \mathbf{r}(\mathbf{h}))]$ under given resource constraints. In particular,

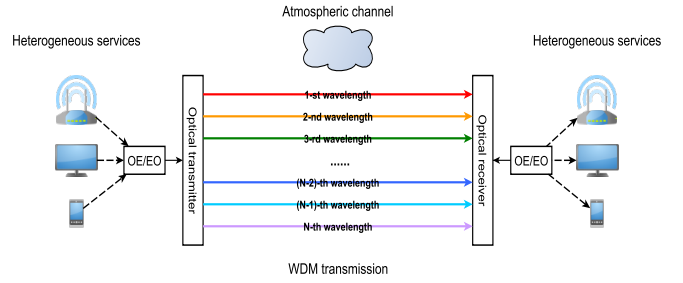


Figure 1. DWDM Radio on Free Space Optics system. The RoFSO transmits multiple RF signals with optical wavelength channels (lines in different colors) simultaneously through atmosphere.

we seek to compute the instantaneous allocated resources $\mathbf{r}(\mathbf{h})$ based on the instantaneous CSI \mathbf{h} , that satisfy required constraints and optimize the system performance. By introducing \mathcal{R} as the action space of allocated resources $\mathbf{r}(\mathbf{h})$, we formulate the optimal resource allocation with the following stochastic optimization problem

$$\begin{aligned} \mathbb{P} &:= \max_{\mathbf{r}(\mathbf{h})} \mathbb{E}_{\mathbf{h}} [f(\mathbf{h}, \mathbf{r}(\mathbf{h}))], \\ \text{s. t. } &\mathbb{E}_{\mathbf{h}} [c_s(\mathbf{r}(\mathbf{h}), f(\mathbf{h}, \mathbf{r}(\mathbf{h})))] \leq 0 \text{ for all } s=1, \dots, S, \\ &\mathbf{r}(\mathbf{h}) \in \mathcal{R}. \end{aligned} \quad (1)$$

We stress in (1) that the objective function $f(\mathbf{h}, \mathbf{r}(\mathbf{h}))$, the constraint functions $c_s(\mathbf{r}(\mathbf{h}), f(\mathbf{h}, \mathbf{r}(\mathbf{h})))$ and the set \mathcal{R} are not necessarily convex or non-convex depending on specific situations. In fact, in most practical cases, they are indeed non-convex given the complexity of FSO systems. In general, the objective function is typically complicated and the allocated resources can be both continuous and discrete, such that solving the resource allocation problem (1) can be difficult. There are mainly four challenges in our concern:

- (i) The objective function $f(\mathbf{h}, \mathbf{r}(\mathbf{h}))$ can be extremely complicated in FSO systems, yielding non-convex optimization problems—see the example in Sections II-A and II-B.
- (ii) The imposed constraints $c_s(\mathbf{r}(\mathbf{h}), f(\mathbf{h}, \mathbf{r}(\mathbf{h})))$ are difficult to address, resulting in failures of conventional optimization algorithms—see the example in Section II-C.
- (iii) The variable to be optimized $\mathbf{r}(\mathbf{h})$ is a function of the channel state information \mathbf{h} and consequently infinite dimensional.
- (iv) FSO systems are sophisticated due to the complexity of optical equipments. Mathematical models $f(\mathbf{h}, \mathbf{r}(\mathbf{h}))$ built for these systems may not be accurate such that model-based algorithms suffer from performance degradations.

In what follows, we first propose a model-based algorithm that solves the problem (1) exactly without any approximation (Section III). We proceed to develop a model-free algorithm via Deep Neural Networks (DNNs) that solves (1) with system observations only, where system models are not required (Section IV). Before proceeding, however, we illustrate in the following subsections how general problem framework in (1)

represents a variety of optimal resource allocation problems in FSO networks.

A. Power Adaptation

We first consider the problem of allocating transmit powers in a Radio on Free Space Optics (RoFSO) system. As a universal platform for heterogeneous wireless services, it transmits RF signals through FSO links in optical networks [37]. The developed Dense Wavelength Division Multiplexing (DWDM) RoFSO system enables simultaneous transmissions of multiple RF signals with WDM technique to increase the transmission capacity. In particular, multimedia RF signals are accessed into the RoFSO system and placed on multiple optical wavelength carriers with optoelectronic devices, and then transmitted into free space. At the receiver, optical signals are received through FSO channels, and transferred back to RF signals for users—See Fig. 1 for system details.

The adaptive transmission is considered when allocating powers to wavelength channels in the RoFSO. Based on the CSI, different powers are assigned to different wavelengths to maximize the total channel capacity. Assume there are N optical wavelength carriers with non-overlapping space between each other. The CSI is represented by the vector $\mathbf{h} = [h_1, \dots, h_N]^T \in \mathbb{R}^N$, where h_i is the CSI of i -th wavelength channel. The allocated power to signal transmitted on i -th wavelength is based upon the observed CSI \mathbf{h} via a power allocation policy $p_i(\mathbf{h})$. Given the collection of power allocations $\mathbf{r}(\mathbf{h}) = [p_1(\mathbf{h}), \dots, p_N(\mathbf{h})]^T \in \mathbb{R}^N$ and the CSI \mathbf{h} , the channel capacity $C_i(\mathbf{h}, \mathbf{r}(\mathbf{h}))$ achieved on i -th wavelength is [20]

$$\begin{aligned} C_i(\mathbf{h}, \mathbf{r}(\mathbf{h})) &= C_i(h_i, p_i(\mathbf{h})) \\ &= \log \left(1 + \frac{\frac{1}{2}(OMI \cdot m_p r p_i(\mathbf{h}) h_i)^2}{RIN \cdot (r p_i(\mathbf{h}) h_i)^2 + 2em_p^{2+F} r p_i(\mathbf{h}) h_i + \frac{4KT}{R_f}} \right) \end{aligned} \quad (2)$$

with OMI the optical modulation index, RIN the relative intensity noise, m_p the photodiode gain, r the photodiode responsivity, e the electric charge, F the excess noise factor, K the Boltzmann's constant, T the temperature and R_f the photodiode resistance. Since different wireless services accessed into the RoFSO have different priorities, we consider the weight vector $\boldsymbol{\omega} = [\omega_1, \dots, \omega_N]^T \in \mathbb{R}^N$ to represent such priorities. The objective function is then the weighted sum of channel capacities over N wavelengths

$$\mathbb{E}_{\mathbf{h}} [f(\mathbf{h}, \mathbf{r}(\mathbf{h}))] = \sum_{i=1}^N \omega_i \mathbb{E}_{\mathbf{h}} [C_i(\mathbf{h}, \mathbf{r}(\mathbf{h}))]. \quad (3)$$

The RoFSO system is further constrained by a total average power limitation P_t at the base station, i.e.

$$\mathbb{E}_{\mathbf{h}} [c(\mathbf{r}(\mathbf{h}))] = \mathbb{E}_{\mathbf{h}} \left[\sum_{i=1}^N p_i(\mathbf{h}) \right] - P_t. \quad (4)$$

Finally, we impose a peak power limitation of P_s for each carrier to ensure eye safety, i.e. $\mathcal{R} = [0, P_s]^N$.

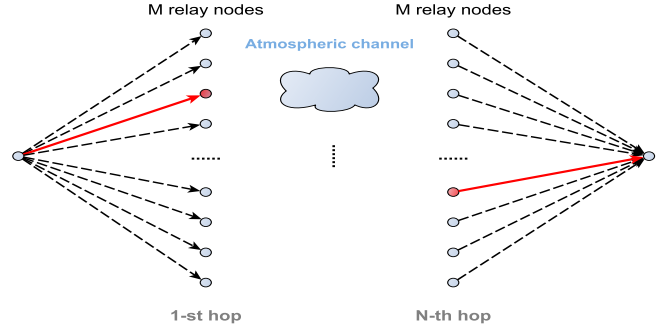


Figure 2. Relay-assisted FSO network. The transmitter communicates with the receiver through multiple selected relays (red nodes).

B. Relay selection

We also consider the relay-assisted FSO network, in which each transmitter communicates with the receiver through intermediate hops. In particular, assume there are N hops where each hop consists of M parallel relays. The transmitter sends the optical signal to a selected relay at 1-st hop. The latter amplifies the received signal and then transmits it to a selected relay at 2-nd hop. The process performs successfully through N hops until the optical signal arrives at the receiver—See Fig. 2 for system details. Based on the CSI, different relays are selected at different hops to maximize the channel capacity. We denote by $\mathbf{h} \in \mathbb{R}^{(M \times N + 2) \times M}$ the CSI between the transmitter, relays and the receiver, and the matrix $\mathbf{r}(\mathbf{h}) = [\boldsymbol{\alpha}_1(\mathbf{h}), \dots, \boldsymbol{\alpha}_N(\mathbf{h})]^T \in \{0, 1\}^{N \times M}$ the selected relays, where each $\boldsymbol{\alpha}_i(\mathbf{h}) = [\alpha_{i1}(\mathbf{h}), \dots, \alpha_{iM}(\mathbf{h})]^T \in \{0, 1\}^M$ is a M -dimensional vector with $\alpha_{ij}(\mathbf{h}) = 1$ if j -th relay is selected at i -th hop and $\alpha_{ij}(\mathbf{h}) = 0$ otherwise. The relay-assisted channel capacity is [28]

$$\begin{aligned} C_{j_1 \dots j_N}(\mathbf{h}) &= \frac{T_f B}{\epsilon} \log \left(1 + \left(\prod_{i=0}^N \left(1 + \frac{1}{P h_{j_i j_{i+1}} \frac{R_g}{e \Delta f}} \right) - 1 \right)^{-1} \right) \end{aligned} \quad (5)$$

which assumes that j_i -th relay is selected at i -th hop and $h_{j_i j_{i+1}}$ is the CSI between j_i -th relay at i -th hop and j_{i+1} -th relay at $(i+1)$ -th hop, where $j_0 = j_{N+1} = 1$ represent the transmitter and the receiver. Here, T_f is the frame duration, B the bandwidth, P the transmission power, R the photodetector sensitivity, g the path loss factor, e the electric charge and Δf the noise equivalent bandwidth. In addition, $\epsilon = 1$ represents the full-duplex relay and $\epsilon = 2$ the half-duplex relay. The objective function is then given by

$$\mathbb{E}_{\mathbf{h}} [f(\mathbf{h}, \mathbf{r}(\mathbf{h}))] = \mathbb{E}_{\mathbf{h}} \left[\sum_{j_N=1}^M \dots \sum_{j_1=1}^M \left(\prod_{i=1}^N \alpha_{ij_i}(\mathbf{h}) \right) C_{j_1 \dots j_N}(\mathbf{h}) \right]. \quad (6)$$

There are N constraints on the selected relays $\mathbf{r}(\mathbf{h})$. That is only one relay can be selected at each hop, i.e., we have

$$\mathcal{R} = \left\{ \{0, 1\}^{N \times M} \mid \sum_{j=1}^M \alpha_{ij}(\mathbf{h}) \leq 1, \text{ for all } i = 1, \dots, N \right\}. \quad (7)$$

Observe that in this example there is no additional stochastic constraint.

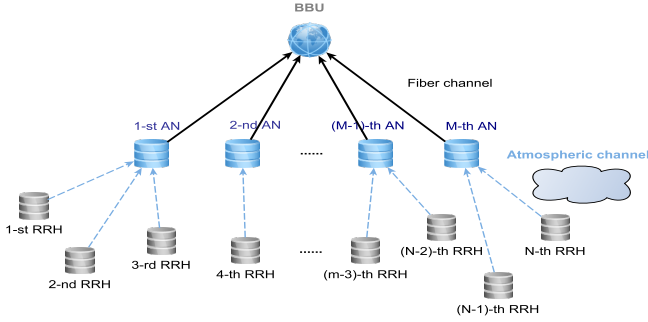


Figure 3. Fronthaul FSO network. RRHs transmit signals with orthogonal optical carriers to their selected ANs through atmosphere, and ANs forward received signals to the BBU. Each link (blue line) between the RRH and the AN contains L orthogonal carrier links.

C. Joint power and relay allocation

The relay selection problem in the previous example can be more complex when considering the joint power adaptation and relay selection, as can be seen in the FSO fronthaul network. As one of cloud radio access network (C-RAN) architectures, it provides high rates, low latency and flexible constructions for 5G wireless networks. In particular, the system consists of remote radio heads (RRHs), aggregation nodes (ANs) and the baseband unit (BBU). The RRHs transmit optical signals with orthogonal optical carriers through free space to the selected ANs. The latter collect received signals and then forward the aggregated signal to the BBU through high speed optical fiber—See Fig. 3 for system details. Based on the CSI, different ANs are selected at different RRHs and different powers are assigned to different optical carriers at each RRH. Assume there are L optical carriers, N RRHs, M ANs and one BBU. The CSI is represented by $\mathbf{h} = \{\mathbf{h}_{ij}\}_{ij}$ for all $i = 1, \dots, N$ and $j = 1, \dots, M$, where each vector $\mathbf{h}_{ij} = [h_{ij}^1, \dots, h_{ij}^L]^\top \in \mathbb{R}^L$ is the CSI of L optical carriers between i -th RRHs and j -th AN. The allocated resources $\mathbf{r}(\mathbf{h}) = \{\mathbf{p}_{ij}(\mathbf{h}), \alpha_{ij}(\mathbf{h})\}_{ij}$ contain assigned powers and selected ANs. Specifically, $\mathbf{p}_{ij}(\mathbf{h}) = [p_{ij}^1(\mathbf{h}), \dots, p_{ij}^L(\mathbf{h})]^\top \in \mathbb{R}^L$ are powers assigned to L optical carriers in the link between i -th RRH and j -th AN, and $\alpha_{ij}(\mathbf{h}) \in \{0, 1\}$ is the indicator being one if j -th AN is selected at i -th RRH and zero otherwise. The channel capacity between i -th RRH and j -th AN is [29]

$$C_{ij}(\mathbf{h}, \mathbf{r}(\mathbf{h})) = \sum_{\ell=1}^L \omega_{\ell} \frac{T_f B}{\epsilon} \log \left(1 + p_{ij}^{\ell}(\mathbf{h}) h_{ij}^{\ell} \frac{Rg}{e\Delta f} \right). \quad (8)$$

with $\boldsymbol{\omega} = [\omega_1, \dots, \omega_L]^\top \in \mathbb{R}^L$ the priorities of optical carriers, T_f the frame duration, B the bandwidth, R the photodetector sensitivity, g the path loss factor, e the electric charge and Δf the noise equivalent bandwidth. The objective function is then the sum of channel capacities over N RRHs

$$\mathbb{E}_{\mathbf{h}} [f(\mathbf{h}, \mathbf{r}(\mathbf{h}))] = \mathbb{E}_{\mathbf{h}} \left[\sum_{i=1}^N \sum_{j=1}^M \alpha_{ij}(\mathbf{h}) C_{ij}(\mathbf{h}, \mathbf{r}(\mathbf{h})) \right]. \quad (9)$$

There are $2N$ constraints for the allocated powers, N constraints for the selected ANs and additional M constraints for the aggregated data at ANs: (i) the total power limitation P_t

and the peak power limitation P_s at each RRH as the example in Section II-A; (ii) only one AN can be selected at each RRH as the example in Section II-B; (iii) the aggregated data traffic shall not exceed the maximal capacity C_t of optical fiber at each AN to avoid the data congestion. Therefore, we have

$$\mathbb{E}_{\mathbf{h}} \left[\sum_{\ell=1}^L p_{ij}^{\ell}(\mathbf{h}) \right] - P_t \leq 0, \text{ for all } i=1, \dots, N, j=1, \dots, M, \quad (10a)$$

$$\mathbb{E}_{\mathbf{h}} \left[\sum_{i=1}^N C_{ij}(\mathbf{h}, \mathbf{r}(\mathbf{h})) \right] - C_t \leq 0, \text{ for all } j=1, \dots, M, \quad (10b)$$

$$\mathcal{R} = \left\{ [0, P_s]^{N \times M \times L} \times \{0, 1\}^{N \times M} \mid \sum_{j=1}^M \alpha_{ij}(\mathbf{h}) \leq 1, \text{ for all } i=1, \dots, N \right\}. \quad (10c)$$

III. STOCHASTIC DUAL GRADIENT ALGORITHM

In this section, we first address three primary challenges (i)-(iii) outlined in Section II by working in the dual domain. In particular, by establishing a null duality gap result for (1), we present the Stochastic Dual Gradient (SDG) algorithm that can find exact solutions despite the non-convexity, constraints, and infinite dimensionality. For the purposes of developing the SDG algorithm, we initially ignore challenge (iv) and assume that models established for FSO systems are accurate—e.g., in the RoFSO system we assume the channel capacity function $C_i(\mathbf{h}, \mathbf{r}(\mathbf{h}))$ in (2) characterizes the RoFSO system accurately.

With a set of convex or non-convex constraints, it is natural to consider working in the dual domain. By introducing the dual variables $\boldsymbol{\lambda} = [\lambda_1, \dots, \lambda_S]^\top \in \mathbb{R}_+^S$ that corresponds to S constraints, the Lagrangian of problem (1) is given by

$$\mathcal{L}(\mathbf{r}(\mathbf{h}), \boldsymbol{\lambda}) = \mathbb{E}_{\mathbf{h}} [f(\mathbf{h}, \mathbf{r}(\mathbf{h}))] - \sum_{s=1}^S \lambda_s \mathbb{E}_{\mathbf{h}} [c_s(\mathbf{r}(\mathbf{h}), f(\mathbf{h}, \mathbf{r}(\mathbf{h})))] \quad (11)$$

Each constraint in (1) shows as a penalty in (11), where the violation is penalized up to a dual variable. We define the dual function as the maximum of Lagrangian

$$\mathcal{D}(\boldsymbol{\lambda}) = \max_{\mathbf{r}(\mathbf{h}) \in \mathcal{R}} \mathcal{L}(\mathbf{r}(\mathbf{h}), \boldsymbol{\lambda}). \quad (12)$$

The problem (12) is unconstrained such that conventional optimization algorithms can be used. With dual variables involved, it has been proved that $\mathcal{D}(\boldsymbol{\lambda}) \geq \mathbb{P}$ holds for any $\boldsymbol{\lambda}$. This result motivates the development of dual problem, that is to find $\boldsymbol{\lambda}^*$ minimizing the dual function

$$\mathbb{D} = \min_{\boldsymbol{\lambda} \geq 0} \mathcal{D}(\boldsymbol{\lambda}) = \min_{\boldsymbol{\lambda} \geq 0} \max_{\mathbf{r}(\mathbf{h}) \in \mathcal{R}} \mathcal{L}(\mathbf{r}(\mathbf{h}), \boldsymbol{\lambda}). \quad (13)$$

The optimal solution \mathbb{D} for (13) can be viewed as the best approximation of \mathbb{P} when handling constraints as penalties. However, it is still unclear how much the difference between \mathbb{D} and \mathbb{P} is and further how to develop an algorithm to solve the alternative min-max problem (13). We consider these issues in following subsections.

A. Null Duality Gap

For the ideal scenario, one would expect the difference $\mathbb{D} - \mathbb{P}$, referred as the duality gap, to be zero. As such, we can solve the general resource allocation problem (1) by solving its associated dual problem (13) without loss of optimality. It is well-known that the null duality gap holds for convex optimization problems. However, the problem (1) in our case is rarely convex due to complicated objective functions and constraints as observed from Sections II-A, II-B and II-C. Solving it in the dual domain then seems to be impossible in principle. Nevertheless, we note the key reason that makes the dual method impractical is not the non-convex property but the existence of duality gap indeed, which leads to the loss of optimality if using the dual method. Put simply, as long as we can show that the problem does have null duality gap, it is feasible to be solved in the dual domain.

Observe that the objective function and constraints in (1) are considered in expectation. Motivated by this observation, we give the following theorem to show its null duality gap.

Theorem 1. [36, Theorem 1] *Let \mathbb{P} and \mathbb{D} be optimal solutions of the primal problem (1) and its associated dual problem (13). Assume that there exists a feasible point \mathbf{r}_0 satisfying all constraints with strict inequality, and the probability distribution of CSI \mathbf{h} contains no point of positive probability. Then we have the null duality gap, i.e., it holds that*

$$\mathbb{P} = \mathbb{D}. \quad (14)$$

Our formulated problem satisfies all conditions required in Theorem 1. As such, we obtain the null duality gap $\mathbb{D} - \mathbb{P} = 0$ even if it is a non-convex optimization problem. We can then focus on the alternative unconstrained problem (13), and develop the dual methodology to solve (1) by solving (13) without any relaxation or approximation.

B. Stochastic Dual Gradient Algorithm

We propose the SDG algorithm based on the above analysis, which iteratively searches for the optimal dual variable $\boldsymbol{\lambda}^*$, starting from an initial iterate $\boldsymbol{\lambda}^0$, to derive the corresponding optimal allocated resource policy $\mathbf{r}^*(\mathbf{h})$. In particular, the SDG consists of two main steps over an iteration index k . The primal step updates the primal variables $\mathbf{r}(\mathbf{h})$ given the current iterate $\boldsymbol{\lambda}^k$, while the dual step updates the dual variables $\boldsymbol{\lambda}$ given the updated $\mathbf{r}^{k+1}(\mathbf{h})$. Details are formally introduced below.

(1) *Primal step.* At k -th iteration given the dual variables $\boldsymbol{\lambda}^k$ and the CSI \mathbf{h} , we update the primal variables by maximizing the Lagrangian as

$$\begin{aligned} \mathbf{r}^{k+1}(\mathbf{h}) &= \underset{\mathbf{r}(\mathbf{h}) \in \mathcal{R}}{\operatorname{argmax}} \mathcal{L}(\mathbf{r}(\mathbf{h}), \boldsymbol{\lambda}^k) \\ &= \underset{\mathbf{r}(\mathbf{h}) \in \mathcal{R}}{\operatorname{argmax}} \mathbb{E}_{\mathbf{h}} [f(\mathbf{h}, \mathbf{r}(\mathbf{h}))] - \sum_{s=1}^S \lambda_s^k \mathbb{E}_{\mathbf{h}} [c_s(\mathbf{r}(\mathbf{h}), f(\mathbf{h}, \mathbf{r}(\mathbf{h})))]. \\ &= \underset{\mathbf{r}(\mathbf{h}) \in \mathcal{R}}{\operatorname{argmax}} f(\mathbf{h}, \mathbf{r}(\mathbf{h})) - \sum_{s=1}^S \lambda_s^k c_s(\mathbf{r}(\mathbf{h}), f(\mathbf{h}, \mathbf{r}(\mathbf{h}))). \end{aligned} \quad (15)$$

Algorithm 1 Stochastic Dual Gradient Algorithm

- 1: **Input:** The objective function $f(\mathbf{h}, \mathbf{r}(\mathbf{h}))$, the constraints $\{c_s(\mathbf{r}(\mathbf{h}), f(\mathbf{h}, \mathbf{r}(\mathbf{h})))\}_{s=1}^S$, the CSI \mathbf{h} and the initial dual variables $\boldsymbol{\lambda}^0$
 - 2: **for** $k = 0, 1, 2, \dots$ **do** {main loop}
 - 3: Update the primal variables
 - 4: $\mathbf{r}^{k+1}(\mathbf{h}) = \underset{\mathbf{r}(\mathbf{h}) \in \mathcal{R}}{\operatorname{argmax}} f(\mathbf{h}, \mathbf{r}(\mathbf{h})) - \sum_{s=1}^S \lambda_s^k c_s(\mathbf{r}(\mathbf{h}), f(\mathbf{h}, \mathbf{r}(\mathbf{h})))$
 - 5: Update the dual variables
 - 6: **for** $s = 1, \dots, S$ **do** {main loop}
 - 7: $\lambda_s^{k+1} = [\lambda_s^k - \eta^k c_s(\mathbf{r}^{k+1}(\mathbf{h}), f(\mathbf{h}, \mathbf{r}^{k+1}(\mathbf{h})))]_+$
 - 8: **end for**
 - 9: **end for**
-

where the last equality is because the expectation is automatically maximized if it is maximized at each sample \mathbf{h} . In practice, (15) can usually be simplified based on specific system models. For example, in the RoFSO system, both the objective function and constraints separate the use of components $p_1(\mathbf{h}), \dots, p_N(\mathbf{h})$ in $\mathbf{r}(\mathbf{h})$ and h_1, \dots, h_N in \mathbf{h} with no coupling between them. Thus, (15) can be simplified to N scalar sub-problems that update each component $p_i(\mathbf{h})$ separately as

$$p_i^{k+1}(\mathbf{h}) = \underset{p_i(\mathbf{h}) \in [0, P_s]}{\operatorname{argmax}} \omega_i C_i(h_i, p_i(\mathbf{h})) - p_i(\mathbf{h}). \quad (16)$$

for all $i = 1, \dots, N$.

(2) *Dual step.* Given the updated $\mathbf{r}^{k+1}(\mathbf{h})$ from step (1), we perform the dual gradient descent to update the dual variables $\boldsymbol{\lambda}^k$

$$\begin{aligned} \lambda_s^{k+1} &= \left[\lambda_s^k - \eta^k \nabla_{\lambda_s} \mathcal{L}(\mathbf{r}^{k+1}(\mathbf{h}), \boldsymbol{\lambda}^k) \right]_+ \\ &= \left[\lambda_s^k - \eta^k c_s(\mathbf{r}^{k+1}(\mathbf{h}), f(\mathbf{h}, \mathbf{r}^{k+1}(\mathbf{h}))) \right]_+ \end{aligned} \quad (17)$$

for all $s = 1, \dots, S$, where η^k is the dual step-size at iteration k and $[\cdot]_+ = \max(\cdot, 0)$ is due to the non-negativity of dual variables $\boldsymbol{\lambda}$.

By repeating these two steps recursively, $\boldsymbol{\lambda}^k$ converges to the optimal values $\boldsymbol{\lambda}^*$ as k increases [38]. Due to the null duality gap result in (14), the optimal solution $\mathbf{r}^*(\mathbf{h})$ can be obtained from $\boldsymbol{\lambda}^*$ as

$$\mathbf{r}^*(\mathbf{h}) = \underset{\mathbf{r}(\mathbf{h}) \in \mathcal{R}}{\operatorname{argmax}} f(\mathbf{h}, \mathbf{r}(\mathbf{h})) - \sum_{s=1}^S \lambda_s^* c_s(\mathbf{r}(\mathbf{h}), f(\mathbf{h}, \mathbf{r}(\mathbf{h}))). \quad (18)$$

Algorithm 1 summarizes the SDG algorithm.

With accurate system models, the SDG algorithm solves the problem (1) perfectly in theory. However, in practice, there exists several problems that make the implementation of the SDG often infeasible. For one thing, observe that, in the primal step of the SDG, there is no closed-form solution of (15) to compute optimal $\mathbf{r}^{k+1}(\mathbf{h})$. Similarly, even after the algorithm converges, real time execution of $\mathbf{r}^*(\mathbf{h})$ in (15) needs to numerically solve a non-convex optimization problem. As such, it may require significant computational complexity.

Apart from the complexity, we recall the difficulty of obtaining accurate system models in FSO systems as stated in challenge (iv) in Section II. Observe that the SDG algorithm heavily depends on exact system models, that is we need accurate knowledge of objective functions $f(\mathbf{h}, \mathbf{r}(\mathbf{h}))$ and constraints $c_s(\mathbf{r}(\mathbf{h}), f(\mathbf{h}, \mathbf{r}(\mathbf{h})))$ to perform this algorithm, which may not be available in practice. This inspires the development of a model-free and low-complexity learning-based algorithm to solve the resource allocation problem, as we introduce in the following section.

IV. PRIMAL-DUAL DEEP LEARNING ALGORITHM

To handle above limitations of the SDG algorithm, we develop the model-free Primal-Dual Deep Learning (PDDL) algorithm. Its implementation requires only observed channel capacities and CSI values with no need of system models. We begin by noticing the optimization problem (1) shares the same structure as the statistical learning problem. This inspires us to introduce a parametrization $\theta \in \mathbb{R}^q$ to represent the resource allocation policy $\mathbf{r}(\mathbf{h})$ by

$$\mathbf{r}(\mathbf{h}) = \Phi(\mathbf{h}, \theta). \quad (19)$$

By substituting (19) into (1), the problem becomes

$$\begin{aligned} \mathbb{P}_\theta := \max_{\theta} \mathbb{E}_{\mathbf{h}} [f(\mathbf{h}, \Phi(\mathbf{h}, \theta))], \\ \text{s. t. } \mathbb{E}_{\mathbf{h}} [c_s(\Phi(\mathbf{h}, \theta), f(\mathbf{h}, \Phi(\mathbf{h}, \theta)))] \leq 0 \text{ for all } s=1, \dots, S, \\ \theta \in \Theta. \end{aligned} \quad (20)$$

where Θ is the set satisfying $\Phi(\mathbf{h}, \theta) \in \mathcal{R}$. The goal is then to learn the optimal function $\Phi^*(\mathbf{h}, \theta^*)$ by finding the optimal parameter vector θ^* that maximizes the objective function while satisfying prescribed constraints.

A. Near-universal Parametrization

The parametrization in (20) inevitably introduces a loss of optimality since resource allocation functions are restricted to those adhered to the form of $\mathbf{r}(\mathbf{h}) = \Phi(\mathbf{h}, \theta)$. For example, with a linear parametrization $\Phi(\mathbf{h}, \theta) = \theta^\top \mathbf{h}$, it is impossible to represent any nonlinear resource allocation policy. A good choice of $\Phi(\mathbf{h}, \theta)$ should provide an accurate approximation for almost all functions in \mathcal{R} by changing parameters θ , and thus can model the space of allowable resource allocations to guarantee the learning performance. To quantify such function representation ability, we define the near-universal parametrization as follows.

Definition 1 (Near-universal parametrization). *For any $\epsilon \geq 0$, the parametrization $\Phi(\mathbf{h}, \theta)$ is ϵ -universal if for any $\mathbf{r}(\mathbf{h}) \in \mathcal{R}$, there exists a set of parameters $\theta \in \Theta$ such that*

$$\mathbb{E}_{\mathbf{h}} [\|\mathbf{r}(\mathbf{h}) - \Phi(\mathbf{h}, \theta)\|_\infty] \leq \epsilon. \quad (21)$$

The universal property has been found in a number of machine learning architectures, e.g., Radial Basis Function Networks (RBFNs) [39], Reproducing Kernel Hilbert Spaces (RKHSs) [40] and Deep Neural Networks (DNNs) [41].

DNNs in particular are well-suited candidates that exhibit the universal function approximation ability and have been

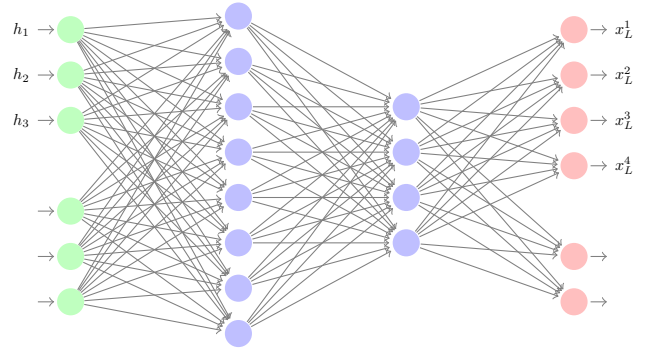


Figure 4. Deep neural network architecture with 2 hidden layers. The channel state information \mathbf{h} is fed into the input units (green nodes), processed by hidden units (blue nodes) and output in the last-layer units (red nodes).

applied successfully in various practical problems. DNNs are the layered architectures that consist of linear operations and pointwise nonlinearities, also referred as activation functions. In particular, consider a DNN with L layers. At each layer ℓ , we have the input feature $\mathbf{x}_{\ell-1} \in \mathbb{R}^{n_{\ell-1}}$ with $n_{\ell-1}$ the number of hidden units at layer $(\ell-1)$. This feature is processed by the linear operation $\mathbf{\Pi}_\ell \in \mathbb{R}^{n_\ell \times n_{\ell-1}}$ to obtain the higher-level feature $\mathbf{u}_\ell \in \mathbb{R}^{n_\ell}$. The latter is passed through a pointwise nonlinearity $\sigma(\cdot) : \mathbb{R} \rightarrow \mathbb{R}$ to generate the output feature

$$\mathbf{x}_\ell = \sigma(\mathbf{\Pi}_\ell \mathbf{x}_{\ell-1}). \quad (22)$$

The output at layer ℓ is then taken as the input at layer $(\ell+1)$. The process repeats recursively until the final layer L —See Fig. 4 for architecture details. With respect to our case, the input of the DNN is the instantaneous CSI $\mathbf{x}_0 = \mathbf{h}$ and the output is $\mathbf{x}_L = \Phi(\mathbf{h}, \theta)$. The parametrization $\theta \in \mathbb{R}^q$ are the weights of linear operations $\mathbf{\Pi}_1, \dots, \mathbf{\Pi}_L$, where $q = \sum_{\ell=0}^{L-1} n_\ell n_{\ell+1}$ is determined by feature dimensions n_0, \dots, n_L . Common examples for the nonlinearity can be the absolute value, the ReLU function, the sigmoid function, etc.

We follow to verify the near-universal property of DNNs. Indeed, DNNs can parametrize arbitrary functions precisely with the increase of the number of layers L and the layer sizes n_ℓ for $\ell = 1, \dots, L$. We formally state this property in the following theorem regarding the universality of DNNs.

Theorem 2. [41, Theorem 2.2] *Let $m(\mathbf{h})$ be the distribution of the channel state information \mathbf{h} and \mathcal{R} the considered set of measurable functions. For a DNN with arbitrarily large number of layers and arbitrarily large layer sizes, it is dense in probability in \mathcal{R} , i.e., for any function $\mathbf{r}(\mathbf{h}) \in \mathcal{R}$ and $\epsilon > 0$, there exists L , $\{n_1, \dots, n_L\}$ and $\theta \in \mathbb{R}^q$ such that*

$$m(\{\mathbf{h} : \|\Phi(\mathbf{h}, \theta) - \mathbf{r}(\mathbf{h})\|_\infty > \epsilon\}) < \epsilon. \quad (23)$$

Theorem 2 establishes that functions in the considered set can be approximated by the DNN parametrization with arbitrarily small accuracy ϵ , validating its near-universal property. Therefore, the parametrization loss $\mathbb{P} - \mathbb{P}_\theta$ can be sufficiently small by learning with the DNN parametrization.

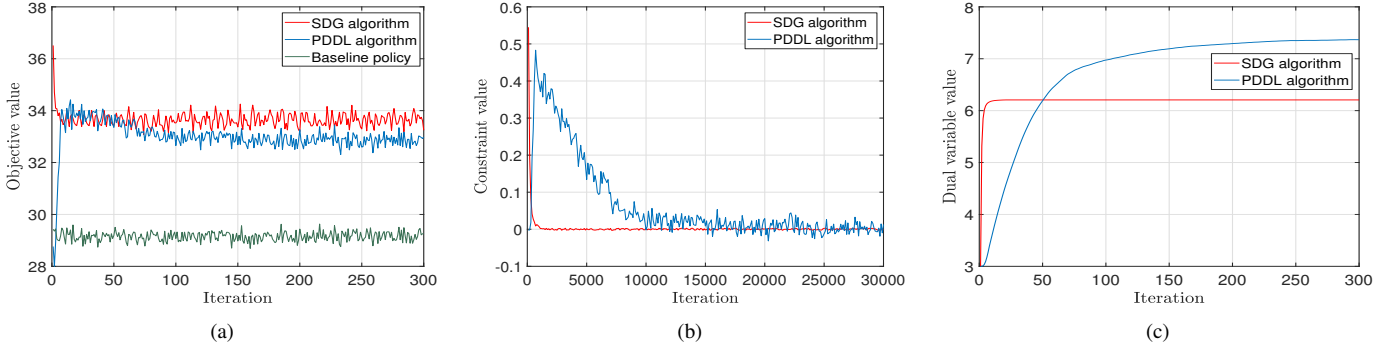


Figure 5. Performance of the SDG algorithm, the PDDL algorithm and the baseline policy for power adaptation in the 10 wavelength multiplexing RoFSO system. (a) The objective value. (b) The constraint value. (c) The dual variable value.

B. Primal-Dual Learning

We proceed to develop an analogous dual-domain method to find the optimal policy parameter θ^* . As in the unparameterized problem, we begin by formulating the Lagrangian of (20) as

$$\begin{aligned} \mathcal{L}(\theta, \lambda) & \quad (24) \\ & = \mathbb{E}_{\mathbf{h}}[f(\mathbf{h}, \Phi(\mathbf{h}, \theta))] - \sum_{s=1}^S \lambda_s \mathbb{E}_{\mathbf{h}}[c_s(\Phi(\mathbf{h}, \theta), f(\mathbf{h}, \Phi(\mathbf{h}, \theta)))]. \end{aligned}$$

The corresponding dual problem is subsequently defined as

$$\mathbb{D}_{\theta} = \min_{\lambda \geq 0} \mathcal{D}_{\theta}(\lambda) = \min_{\lambda \geq 0} \max_{\theta \in \Theta} \mathcal{L}(\theta, \lambda). \quad (25)$$

For the above min-max problem with the parametrization θ , the duality gap $\mathbb{P}_{\theta} - \mathbb{D}_{\theta}$ grows in inverse proportion to the function approximation ability [35]. Since the DNN is near-universal as shown in Theorem 2, the duality gap is sufficiently close to null such that we can solve (25) with little loss of optimality.

We then develop the Primal-Dual Deep Learning (PDDL) algorithm for (25), which updates the primal variables θ and the dual variables λ simultaneously at each iteration with gradient descents. Specifically, we follow two steps at each iteration k :

(1) *Primal step.* Given the dual variables λ^k and the CSI \mathbf{h} , we update the primal variables θ as

$$\begin{aligned} \theta^{k+1} & = \theta^k + \delta^k \nabla_{\theta} \mathcal{L}(\theta^k, \lambda^k) \\ & = \theta^k + \delta^k \nabla_{\theta} \mathbb{E}_{\mathbf{h}}[f(\mathbf{h}, \Phi(\mathbf{h}, \theta))] - \sum_{s=1}^S \lambda_s c_s(\Phi(\mathbf{h}, \theta), f(\mathbf{h}, \Phi(\mathbf{h}, \theta))) \end{aligned} \quad (26)$$

where δ^k is the primal step-size at iteration k , and the last equation is due to the linearity of the expectation.

(2) *Dual step.* Given the updated θ^{k+1} from step (1), the dual variables λ is updated similarly

$$\lambda_s^{k+1} = \left[\lambda_s^k - \eta^k \mathbb{E}_{\mathbf{h}}[c_s(\Phi(\mathbf{h}, \theta^{k+1}), f(\mathbf{h}, \Phi(\mathbf{h}, \theta^{k+1}))) \right]_+ \quad (27)$$

for all $s = 1, \dots, S$, where η^k is the dual step-size.

The PDDL algorithm learns the optimal primal and dual variables θ^* and λ^* by recursively repeating primal and dual steps. Observe that the primal-dual algorithm used in the parameterized problem features a closed form update in (26), in

Algorithm 2 Primal-Dual Deep Learning Algorithm

- 1: **Input:** Initial primal and dual variables θ^0, λ^0
 - 2: **for** $k = 0, 1, 2, \dots$ **do** {main loop}
 - 3: Draw CSI samples $\{\mathbf{h}_{\tau}\}_{\tau=1}^{\mathcal{T}}$ of batch-size \mathcal{T} , and get their corresponding $\{\mathbf{r}_{\tau}\}_{\tau=1}^{\mathcal{T}}$ according to DNN outputs $\{\Phi(\mathbf{h}_{\tau}, \theta^k)\}_{\tau=1}^{\mathcal{T}}$ and policy distributions $\{\pi_{\mathbf{h}_{\tau}, \theta^k}(\mathbf{r})\}_{\tau=1}^{\mathcal{T}}$
 - 4: Obtain observations of objective function $\{f(\mathbf{r}_{\tau}, \mathbf{h}_{\tau})\}_{\tau=1}^{\mathcal{T}}$ at current samples $\{\mathbf{h}_{\tau}\}_{\tau=1}^{\mathcal{T}}$
 - 5: Compute the policy gradient $\widetilde{\nabla}_{\theta} \mathcal{L}(\theta^k, \lambda^k)$ by (30)
 - 6: Update the primal variables by (26)
 $\theta^{k+1} = \theta^k + \delta^k \widetilde{\nabla}_{\theta} \mathcal{L}(\theta^k, \lambda^k)$
 - 7: Update the dual variables by (27)
 $\lambda^{k+1} = \left[\lambda^k - \eta^k \nabla_{\lambda} \mathcal{L}(\theta^{k+1}, \lambda^k) \right]_+$
 - 8: **end for**
-

contrast to the computationally expensive inner maximization required in (15) at each step of the SDG algorithm used in the unparameterized problem. Even still, direct evaluation of the primal update in (26) requires the knowledge of system models to evaluate the expected values and gradients, generally not available in practice. However, unlike the SDG algorithm, the PDDL algorithm is capable of leveraging the so-called policy gradient method to develop a completely model-free algorithm as detailed in the next subsection.

C. Model-Free Policy Gradient

Policy gradient has been developed as a practical gradient estimation method in reinforcement learning. It exploits a likelihood ratio property to compute the gradient for policy functions taking the form of $\mathbb{E}_{\mathbf{h}}[f(\Phi(\mathbf{h}, \theta), \mathbf{h})]$, where $f(\cdot)$ is unknown. Put simply, it provides a stochastic and model-free approximation for $\nabla_{\theta} \mathbb{E}_{\mathbf{h}}[f(\Phi(\mathbf{h}, \theta), \mathbf{h})]$ [42].

In particular, we consider the policy function $\Phi(\mathbf{h}, \theta)$ as stochastic realizations drawn from a distribution with the delta density function $\pi_{\mathbf{h}, \theta}(\mathbf{r}) = \delta(\mathbf{r} - \Phi(\mathbf{h}, \theta))$. We can then rewrite the Jacobian of the policy function as

$$\nabla_{\theta} \mathbb{E}_{\mathbf{h}}[f(\mathbf{h}, \Phi(\mathbf{h}, \theta))] = \mathbb{E}_{\mathbf{h}, \mathbf{r}}[f(\mathbf{h}, \mathbf{r}) \nabla_{\theta} \log \pi_{\mathbf{h}, \theta}(\mathbf{r})], \quad (28)$$

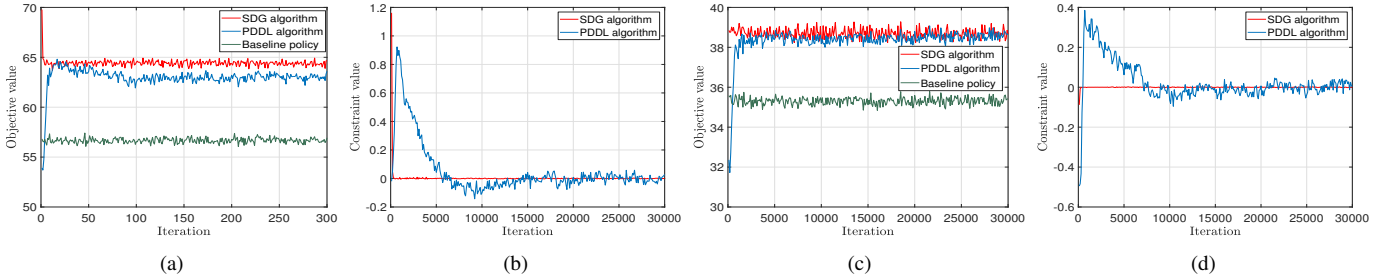


Figure 6. Performance of the SDG algorithm, the PDDL algorithm and the baseline policy for power adaptation in different RoFSO system configurations. (a) The objective value for 20 wavelength multiplexing with power limitations $P_t = 3W$, $P_s = 0.3W$. (b) The constraint value for 20 wavelength multiplexing with power limitations $P_t = 3W$, $P_s = 0.3W$. (c) The objective value for 10 wavelength multiplexing with power limitations $P_t = 3W$, $P_s = 0.6W$. (d) The constraint value for 10 wavelength multiplexing with power limitations $P_t = 3W$, $P_s = 0.6W$.

where \mathbf{r} is a random realization drawn from the distribution $\pi_{\mathbf{h},\theta}(\mathbf{r})$. We now translate the computation of $\nabla_{\theta} \mathbb{E}_{\mathbf{h}}[f(\mathbf{h}, \Phi(\mathbf{h}, \theta))]$ to a function evaluation $f(\mathbf{h}, \mathbf{r})$ multiplied with the gradient of the density function $\nabla_{\theta} \log \pi_{\mathbf{h},\theta}(\mathbf{r})$. However, computing $\nabla_{\theta} \log \pi_{\mathbf{h},\theta}(\mathbf{r})$ for a delta density function still requires the knowledge of $f(\cdot)$ and $m(\mathbf{h})$. We further address this issue by approximating the delta function with a known density function centered around $\Phi(\mathbf{h}, \theta)$, such as Gaussian distribution, Binomial distribution, etc. Then we can estimate the gradient of policy function $\nabla_{\theta} \mathbb{E}_{\mathbf{h}}[f(\mathbf{h}, \Phi(\mathbf{h}, \theta))]$ by using (28) without the information of $f(\cdot)$. In addition, we observe \mathcal{T} samples of the CSI and take the average to estimate the expectation $\mathbb{E}_{\mathbf{h}}[\cdot]$

$$\widetilde{\nabla}_{\theta} \mathbb{E}_{\mathbf{h}}[f(\mathbf{h}, \Phi(\mathbf{h}, \theta))] = \frac{1}{\mathcal{T}} \sum_{\tau=1}^{\mathcal{T}} f(\mathbf{h}_{\tau}, \mathbf{r}_{\tau}) \nabla_{\theta} \log \pi_{\mathbf{h}_{\tau}, \theta}(\mathbf{r}_{\tau}) \quad (29)$$

where \mathbf{h}_{τ} is a sampled CSI and \mathbf{r}_{τ} is a realization drawn from the policy distribution $\pi_{\mathbf{h}_{\tau}, \theta}(\mathbf{r})$. With the use of (29), we can compute the gradient of policy function in (26) as

$$\begin{aligned} \widetilde{\nabla}_{\theta} \mathcal{L}(\theta, \lambda) & \quad (30) \\ &= \widetilde{\nabla}_{\theta} \mathbb{E}_{\mathbf{h}} \left[f(\mathbf{h}, \Phi(\mathbf{h}, \theta)) - \sum_{s=1}^S \lambda_s c_s(\Phi(\mathbf{h}, \theta), f(\mathbf{h}, \Phi(\mathbf{h}, \theta))) \right] \\ &= \frac{1}{\mathcal{T}} \sum_{\tau=1}^{\mathcal{T}} \left\{ \left[f(\mathbf{h}_{\tau}, \mathbf{r}_{\tau}) - \sum_{s=1}^S \lambda_s c_s(\mathbf{r}_{\tau}, f(\mathbf{h}_{\tau}, \mathbf{r}_{\tau})) \right] \nabla_{\theta} \log \pi_{\mathbf{h}_{\tau}, \theta}(\mathbf{r}_{\tau}) \right\} \end{aligned}$$

such that the primal step can be performed in a model-free manner as well as the dual step.

Overall, the PDDL algorithm learns the optimal resource allocation by updating the primal and dual variables without requiring any explicit knowledge of objective functions or CSI distributions, but only their observations. By replacing $\nabla_{\theta} \mathcal{L}(\theta^k, \lambda^k)$ with $\widetilde{\nabla}_{\theta} \mathcal{L}(\theta^k, \lambda^k)$ in (26), the PDDL algorithm is summarized in Algorithm 2.

V. NUMERICAL EXPERIMENTS

In this section, we test the Stochastic Dual Gradient and Primal-Dual Deep Learning algorithms in a number of resource allocation applications in FSO networks to corroborate theory. We consider the average power allocation and/or random relay selection as the baseline policy for performance comparison. For our simulations, the channel state information

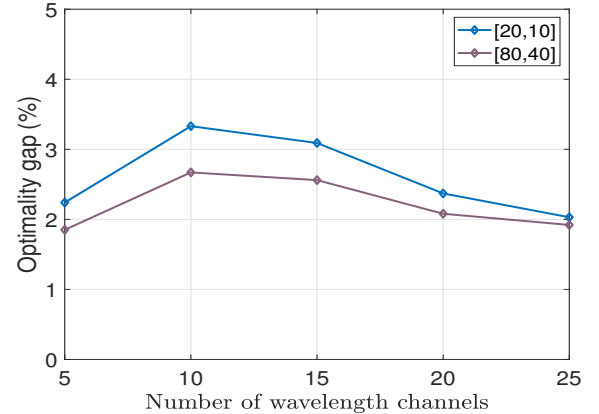


Figure 7. The optimality gap between the SDG algorithm and the PDDL algorithm under different numbers of wavelength channels.

is modelled as the well-known log-normal distribution, which is commonly used under weak-to-moderate turbulence. Without loss of generality, other distributions (e.g., Gamma-Gamma distribution) are also applicable based on practical turbulence conditions. To implement the algorithms, we consider a batch-size of 64 samples. The ADAM optimizer is used for the primal update and the exponentially decaying step-size is used for the dual update. Furthermore, we address the feasibility condition $\mathbf{r}(\mathbf{h}) \in \mathcal{R}$ or $\theta \in \Theta$ in the PDDL algorithm by selecting suitable policy distributions $\pi_{\mathbf{h},\theta}$, as detailed in specific applications.

A. Power Adaptation

We first consider the power adaptation in WDM RoFSO systems—see the example in Section II-A for details [20]. The goal is to allocate powers to orthogonal optical carriers that maximizes the weighted sum-capacity. In particular, the RoFSO transmits multiple signals simultaneously in different wavelength channels and we wish to allocate powers on these channels within total and peak power constraints. The optimization problem can be formulated as

$$\begin{aligned} \mathbb{P} &:= \max_{\mathbf{r}(\mathbf{h})} \sum_{i=1}^N \omega_i \mathbb{E}_{\mathbf{h}} [C_i(\mathbf{h}, \mathbf{r}(\mathbf{h}))], \quad (31) \\ \text{s. t.} & \quad \mathbb{E}_{\mathbf{h}} \left[\sum_{i=1}^N p_i(\mathbf{h}) \right] - P_t \leq 0, \quad \mathcal{R} = [0, P_s]^N \end{aligned}$$

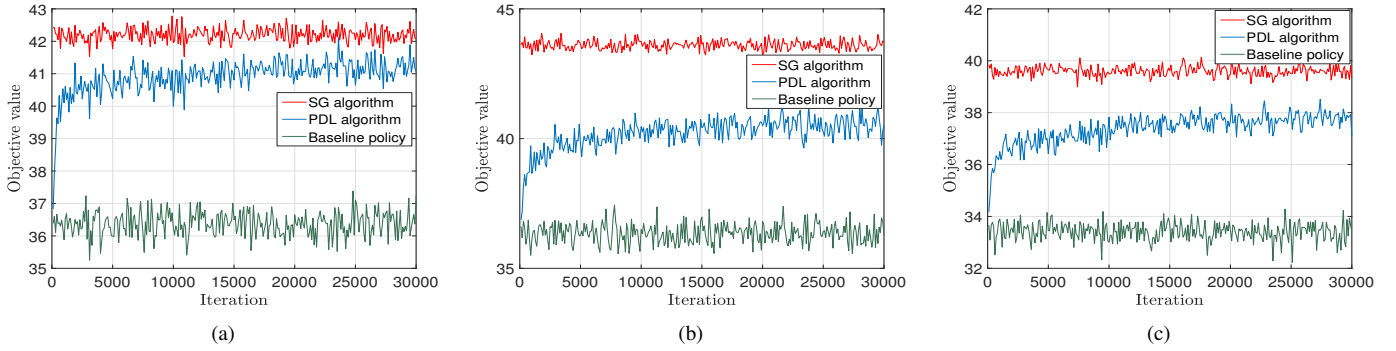


Figure 8. Performance of the SG algorithm, the PDL algorithm and the baseline policy for relay selection in the relay-assisted FSO network. (a) The objective value for 2-hop FSO network with 5 parallel relays per hop. (b) The objective value for 2-hop FSO network with 10 parallel relays per hop. (c) The objective value for 3-hop FSO network with 5 parallel relays per hop.

with $C_i(\mathbf{h}, \mathbf{r}(\mathbf{h}))$ the capacity of i -th wavelength channel [cf. (2)], $\mathbf{r}(\mathbf{h}) = [p_1(\mathbf{h}), \dots, p_N(\mathbf{h})]^\top$ the allocated powers, P_t the total power limitation and P_s the peak power limitation. The problem is challenging due to the complicated objective function and constraints.

In this problem, we consider the policy distribution $\pi_{\mathbf{h}, \theta}$ in the PDDL algorithm as a truncated Gaussian distribution to satisfy the feasibility condition $\mathbf{r}(\mathbf{h}) \in \mathcal{R} = [0, P_s]^N$, i.e., the truncated Gaussian distribution has fixed support on the interval $[0, P_s]$. The output of the DNN $\Phi(\mathbf{h}, \theta) \in \mathbb{R}^{2N}$ is a set of N means and standard deviations that specify N truncated Gaussian distributions. Since there is no coupling or interference between wavelength channels, we construct N independent DNNs serving for N channels. The input of each DNN is the CSI on its associated channel. Each DNN is built with two hidden layers, each of which contains 20 and 10 units respectively. The nonlinearity is the ReLU function $\sigma(\cdot) = [\cdot]_+$.

Fig. 5 shows results of a relatively simple experiment with $N = 10$ wavelength channels. Priority weights $\omega = [\omega_1, \dots, \omega_N]^\top$ are drawn randomly from 0 to 1 and parameters are set as: $P_t = 1.5W$; $P_s = 0.3W$; $m_p = 5$; $OMI = 15\%$; $r = 0.75$; $RIN = -140\text{dB}/\text{Hz}$; $T = 300\text{K}$; transmitter aperture diameter $D_{tx} = 0.015\text{m}$; receiver aperture diameter $D_{rx} = 0.05\text{m}$ and $d = 1000\text{m}$. From Fig. 5a, we see that both the SDG and the PDDL converge as the iteration increases, and outperform the baseline policy. The SDG solves the problem exactly and thus exhibits the best performance. The objective value achieved by the PDDL converges closely to that of the SDG, indicating its near perfect performance. Fig. 5b shows that the constraint value converges to zero with the increase of iteration. This implies the feasibility of solutions obtained by our algorithms. In Fig. 5c, we observe the dual variable learned by the PDDL also converges closely to that of the SDG, where the difference reveals the reason of optimality loss. Finally, we remark that the SDG is model-based that requires the knowledge of RoFSO system models, while the PDDL is completely model-free that is particularly useful when these models are unknown, inaccurate, or too complicated to address. Furthermore, the SDG numerically solves a local maximization problem (16) at each primal update, that is computationally more expensive.

In Fig. 6, we run experiments under different system config-

urations; namely, different number of wavelength channels and different power budgets, to show the algorithm adaptability to changing scenarios. Fig. 6a and Fig. 6b plot the objective and the constraint in the RoFSO system with $N = 20$ wavelength multiplexing. Both the SDG and the PDDL exhibit strong performance, and their performance improvements compared to the baseline policy are emphasized in this larger system. In Fig. 6c and Fig. 6d, we show the performance of three policies in a system with larger power budgets $P_t = 3W$ and $P_s = 0.6W$. Similar results apply here that the SDG and the PDDL outperform the baseline policy. We note that the PDDL converges roughly to the same value as the SDG in this case. This is because the increased power budgets create more space for the PDDL algorithm to manipulate powers, such that the learning ability of the DNN is fully utilized.

To provide a more thorough comparison of the PDDL to the SDG, we perform a series of experiments for changing numbers of channels from 5 to 25 and with different DNN architectures in Fig. 7. In particular, let \mathbb{P} and \mathbb{P}_θ be the sum-capacities achieved by the SDG and the PDDL and we define the normalized optimality gap between two algorithms as

$$\gamma = \frac{\mathbb{P} - \mathbb{P}_\theta}{\mathbb{P}}. \quad (32)$$

We consider two DNN architectures: a small one with hidden layers of size 20 and 10 and a dense one with hidden layers of size 80 and 40. We see that the optimality gap maintains in the low value even for large wavelength multiplexing systems, indicating the near-optimal performance of the PDDL. The dense DNN performs better and is more stable to changing scenarios. This is because the dense architecture improves the learning ability of the DNN, and thus reduces the optimality loss of the PDDL to the SDG.

B. Relay Selection

We then consider the relay selection in relay-assisted FSO networks—see the example in Section II-B for details [28]. In particular, the source transmits optical signals to the receiver through intermediate hops, where each hop contains multiple parallel relays. The goal is to select the appropriate relay at

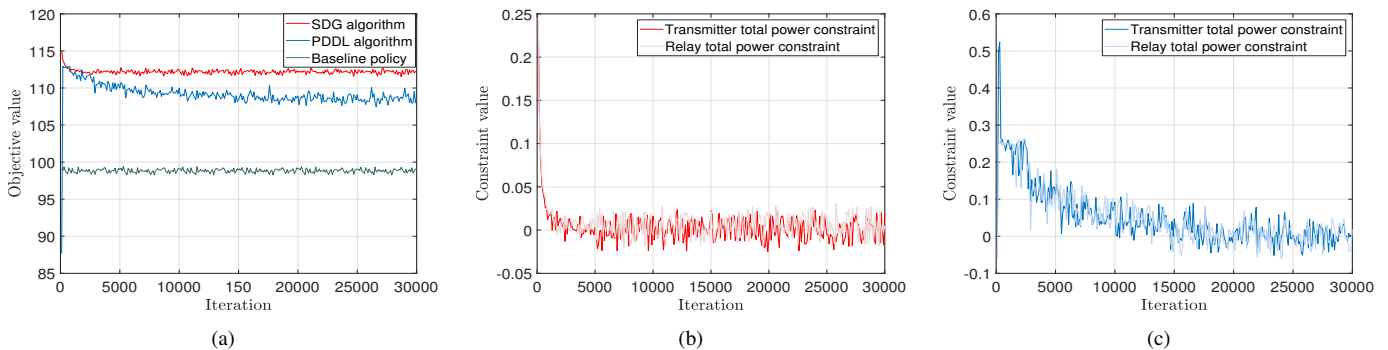


Figure 9. Performance of the SDG algorithm, the PDDL algorithm and the baseline policy for power and relay allocation in the 1-hop relay-assisted multichannel FSO network with 5 parallel relays per hop and 5 orthogonal optical carrier. (a) The objective value. (b) The constraint values for the SDG algorithm. (c) The constraint values for the PDDL algorithm.

each hop to maximize the channel capacity. The optimization problem can be formulated as

$$\mathbb{P} := \max_{\mathbf{r}(\mathbf{h})} \mathbb{E}_{\mathbf{h}} \left[\sum_{j_N=1}^M \cdots \sum_{j_1=1}^M \left(\prod_{i=1}^N \alpha_{ij_i}(\mathbf{h}) \right) C_{j_1 \dots j_N}(\mathbf{h}) \right], \quad (33)$$

$$\text{s. t. } \mathcal{R} = \left\{ \{0, 1\}^{N \times M} \mid \sum_{j=1}^M \alpha_{ij}(\mathbf{h}) \leq 1, \text{ for all } i = 1, \dots, N \right\}.$$

where $C_{j_1 \dots j_N}(\mathbf{h})$ is the channel capacity of the relaying link in which j_i -th relay is selected at i -th hop [cf. (34)], and $\mathbf{r}(\mathbf{h}) = [\alpha_1(\mathbf{h}), \dots, \alpha_N(\mathbf{h})]^T \in \{0, 1\}^{N \times M}$ are selected relays in which $\alpha_i(\mathbf{h}) = [\alpha_{i1}(\mathbf{h}), \dots, \alpha_{iM}(\mathbf{h})]^T \in \{0, 1\}^M$ is a M -dimensional vector with $\alpha_{ij_i}(\mathbf{h}) = 1$ if j_i -th relay is selected at i -th hop and $\alpha_{ij_i}(\mathbf{h}) = 0$ otherwise. It should be noted that there is no stochastic constraint in relay selection, i.e., there is no constraint taking the form of $\mathbb{E}_{\mathbf{h}}[c_s(\mathbf{r}(\mathbf{h}), f(\mathbf{h}, \mathbf{r}(\mathbf{h})))] \leq 0$ in problem (33), in which case the dual update is not actually required. The Stochastic Dual Gradient algorithm then reduces to the Stochastic Gradient (SG) algorithm and the primal-dual deep learning algorithm reduces to the Primal Deep Learning (PDL) algorithm, respectively.

Since the allocated resources are binary variables $\mathbf{r}(\mathbf{h}) \in \mathcal{R}$, we select the policy distribution $\pi_{\mathbf{h}, \theta}$ in the PDL algorithm as the categorical distribution. The categorical distribution describes the possible results as a random variable that takes on one of M possible categories. The outputs of the DNN $\Phi(\mathbf{h}, \theta) \in \mathbb{R}^{N \times M}$ specify the selected probabilities of each category (relay) at each hop. In this problem, the relay selection depends on the CSI over the whole network. We construct a single two-layered DNN of size 200 and 100 hidden units and the nonlinearity is the ReLU function. Channel conditions \mathbf{h} are given as inputs to the DNN, which outputs NM Bernoulli probabilities associated to each relay and hop.

Fig. 8a shows the performance of the SG algorithm, the PDL algorithm and the baseline policy in a 2-hop relay-assisted network. We consider $N = 5$ parallel relays at each hop and assume system parameters as $B = 10^9 \text{ Hz}$, $T_f = 10^{-8} \text{ s}$, $\epsilon = 1$, $P = 0.3 \text{ W}$ and $R = 0.75 \text{ A/W}$. We see that both algorithms converge to stationary points and outperform the baseline policy as expected. The SG performs best on the premise that system models are available at hand. The

PDL follows closely with a similar objective value, which is obtained without explicit model information. We note that the constraints of relay selection are automatically satisfied by using the categorical distribution, confirming the feasibility of obtained solutions.

We continue to perform the algorithms on systems with changing scenarios. We consider the 2-hop network with $N = 10$ relays per hop in Fig. 8b and the 3-hop network with $N = 5$ relays per hop in Fig. 8c. In general, the SG and the PDL perform better than the baseline policy in both scenarios indicating their adaptivity to large FSO networks. On the one hand, the PDL gets slightly degraded compared to the result in Fig. 8a. This follows our intuition because the problem becomes more difficult as we enlarge the system with more relays or more hops, while the DNN architecture keeps same with unchanged expressive power. On the other hand, the SG solves the problem exactly maintaining good performance, while its implementation requires more expensive computations in these cases.

C. Joint Power and Relay allocation (A)

We finally consider the joint power and relay allocation in two applications. In the first experiment, we consider the relay-assisted multichannel FSO network where the system transmits signals with L orthogonal optical carriers through N intermediate hops [28]. In particular, the transmitter modulates signals onto optical carriers and sends these signals simultaneously to the selected relay. The latter aggregates received signals, modulates orthogonal carriers, and transmits them to the selected relay at next hop. The system performs this process recursively until the receiver. We assume there is no crosstalk between orthogonal optical carriers and each hop contains M parallel relays for selection. Based on the CSI, different relays are selected at different hops and different powers are assigned to different carriers at the transmitter and selected relays, in order to maximize the total channel capacity. Let \mathbf{h} be the CSI between the transmitter, relays and the receiver, and $\mathbf{r}(\mathbf{h}) = \{\mathbf{p}_{ij}(\mathbf{h}), \alpha_{ij}(\mathbf{h})\}_{i=0, \dots, N, j=1, \dots, M}$ the allocated resources including assigned powers and selected relays. In particular, $\mathbf{p}_{ij}(\mathbf{h}) = [p_{ij}^1(\mathbf{h}), \dots, p_{ij}^L(\mathbf{h})]^T \in \mathbb{R}^L$ are powers of L optical carriers at j -th relay of i -th hop where $i = 0, j = 1$ and $i = N + 1, j = 1$ represent the transmitter and the receiver, and $\alpha_{ij} \in \{0, 1\}$ indicates whether j -th relay

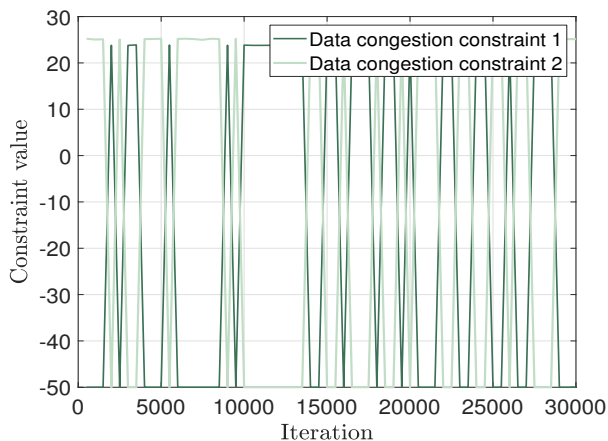


Figure 10. The data congestion constraint values of the baseline policy in the FSO fronthaul network with 5 RRHs, 2 ANs, one BBU and 5 orthogonal carriers.

is selected at i -th hop. The channel capacity of ℓ -th orthogonal channel over a specific selected relaying link is

$$C_{j_1 \dots j_N}^\ell(\mathbf{h}) = \frac{T_f B}{\epsilon} \log \left(1 + \left(\prod_{i=0}^N \left(1 + \frac{1}{p_{i j_i}^\ell(\mathbf{h}) h_{j_i j_{i+1}}^\ell \frac{R q}{e \Delta f}} \right) - 1 \right)^{-1} \right) \quad (34)$$

where we assume j_i -th relay is selected at i -th hop and $h_{j_i j_{i+1}}^\ell$ is the CSI of ℓ -th carrier between j_i -th relay at i -th hop and j_{i+1} -th relay at $(i+1)$ -th hop. Since there is single transmitter and single receiver, we have $j_0 = j_{N+1} = 1$ by default.

We assume three kinds of constraints in this problem: the total power limitation P_t at the transmitter and selected relays, the peak power limitation P_s for each carrier, and that only one relay is selected at each hop. The optimization problem can then be formulated as

$$\begin{aligned} \mathbb{P} := & \max_{\mathbf{r}(\mathbf{h})} \mathbb{E}_{\mathbf{h}} \left[\sum_{j_N=1}^M \cdots \sum_{j_1=1}^M \left(\prod_{i=1}^N \alpha_{i j_i}(\mathbf{h}) \right) \sum_{\ell=1}^L C_{j_1 \dots j_N}^\ell(\mathbf{h}) \right], \quad (35) \\ \text{s. t. } & \mathbb{E}_{\mathbf{h}} \left[\sum_{\ell=1}^L p_{i j_i}^\ell(\mathbf{h}) \right] - P_t \leq 0, \quad i=1, \dots, N, j_i=1, \dots, M, \\ & \mathcal{R} = \left\{ [0, P_s]^{(1+N \times M) \times L} \times \{0, 1\}^{N \times M} \mid \sum_{j_i=1}^M \alpha_{i j_i}(\mathbf{h}) \leq 1, i=1, \dots, N \right\}. \end{aligned}$$

The problem indeed can be considered as the extension of the problem in Section II-B to the scenario with orthogonal optical carriers. The problem is difficult since the objective function is non-convex and the allocated resources include both continuous and binary variables.

We consider the truncated Gaussian distribution for the policy distribution of allocated powers and the categorical distribution for selected relays. The DNN is constructed as a two-layered architecture of size 200 and 100 hidden units with the ReLU nonlinearity. The CSI \mathbf{h} are fed as inputs to the DNN, which outputs parameters that specify policy distributions $\pi_{\mathbf{h}, \theta}$. We consider the 1-hop network with $M = 5$ parallel relays per hop. There are $L = 5$ orthogonal optical

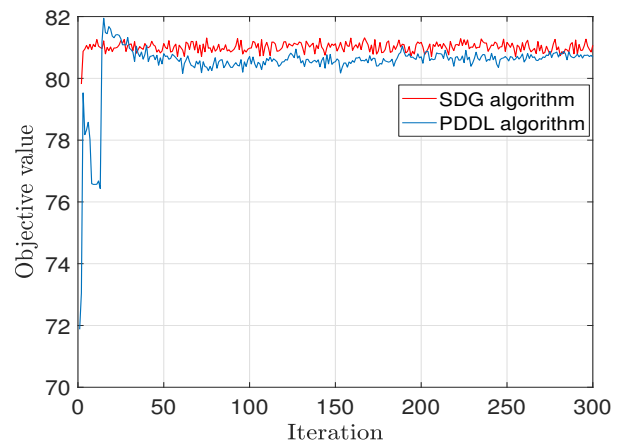


Figure 11. The objective values of the SDG algorithm and the PDDL algorithm in the FSO fronthaul network with 5 RRHs, 2 ANs, one BBU and 5 orthogonal carriers.

carriers at the transmitter and the selected relay, and system parameters are set as: $B = 10^9 \text{ Hz}$, $T_f = 10^{-8} \text{ s}$, $\epsilon = 1$, $P_t = 1.5 \text{ W}$, $P_s = 0.6 \text{ W}$ and $R = 0.75 \text{ A/W}$.

Fig. 9 plots the objective and constraints of the SDG algorithm, the PDDL algorithm and the baseline policy. We observe that performance of the SDG and the PDDL is superior to that of the baseline policy, and performance improvements get emphasized compared to either single power adaptation in Section V-A or single relay selection in Section V-B. This is because advantages of our algorithms get compounded in this joint problem. The PDDL obtains close performance to the SDG but does not require any system model to implement. From Fig. 9b and Fig. 9c, we see that constraint values converge to zero as the iteration increases for both the SDG and the PDDL algorithms, which confirms that the obtained solutions are indeed feasible.

D. Joint Power and Relay allocation (B)

The second experiment in terms of the joint power and relay allocation considers FSO fronthaul networks—see the example in Section II-C for details [29]. In particular, the RRHs transmit signals with orthogonal optical carriers to their selected ANs. The ANs aggregate received signals and then forward to the BBU. The goal is to allocate powers to optical carriers and select the best AN at each RRH that maximizes the sum-capacity. The optimization problem is formulated as

$$\begin{aligned} \mathbb{P} := & \max_{\mathbf{r}(\mathbf{h})} \mathbb{E}_{\mathbf{h}} \left[\sum_{i=1}^N \sum_{j=1}^M \alpha_{i j}(\mathbf{h}) C_{i j}(\mathbf{h}, \mathbf{r}(\mathbf{h})) \right], \quad (36) \\ \text{s. t. } & \mathbb{E}_{\mathbf{h}} \left[\sum_{\ell=1}^L p_{i j}^\ell(\mathbf{h}) \right] - P_t \leq 0, \quad \text{for all } i=1, \dots, N, j=1, \dots, M, \\ & \mathbb{E}_{\mathbf{h}} \left[\sum_{i=1}^N C_{i j}(\mathbf{h}, \mathbf{r}(\mathbf{h})) \right] - C_t \leq 0, \quad \text{for all } j=1, \dots, M, \\ & \mathcal{R} = \left\{ [0, P_s]^{N \times M \times L} \times \{0, 1\}^{N \times M} \mid \sum_{j=1}^M \alpha_{i j}(\mathbf{h}) \leq 1, i=1, \dots, N \right\}. \end{aligned}$$

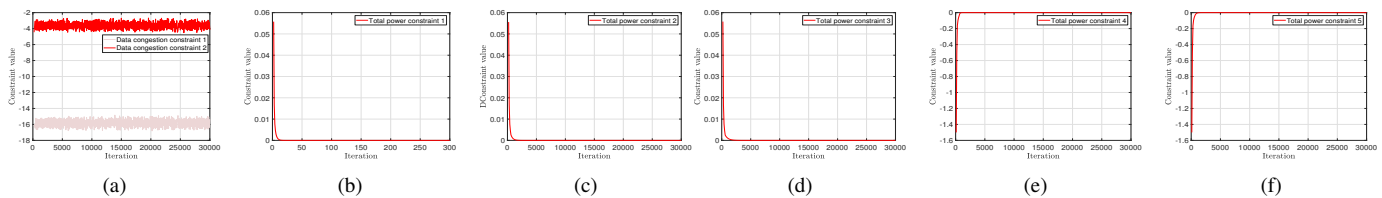


Figure 12. The constraint values of the SDG algorithm in the FSO fronthaul network with 5 RRHs, 2 ANs, one BBU and 5 orthogonal carriers. (a) The data congestion constraints at 2 ANs. (b)-(f) The total power constraints at 5 RRHs.

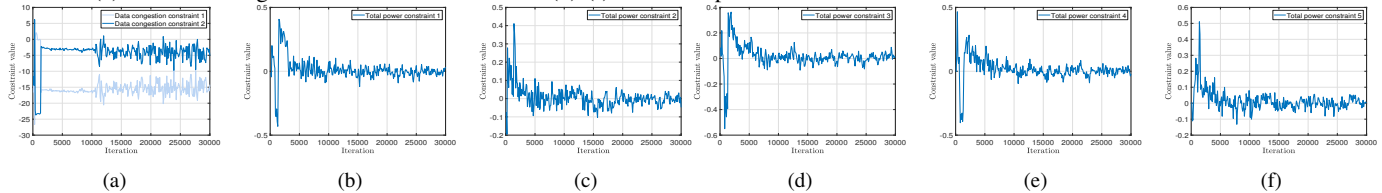


Figure 13. The constraint values of the PDDL algorithm in the FSO fronthaul network with 5 RRHs, 2 ANs, one BBU and 5 orthogonal carriers. (a) The data congestion constraints at 2 ANs. (b)-(f) The total power constraints at 5 RRHs.

We note that the data congestion constraints further complicate the problem, making it extremely difficult to solve in practice.

We similarly consider the truncated Gaussian distribution and the categorical distribution for policy distributions of allocated powers and selected relays, respectively. Since the problem becomes more complicated, we consider a denser DNN with 3 layers, each of which contains 400, 200 and 100 hidden units. The ReLU nonlinearity is used. The inputs are all channel conditions \mathbf{h} over network and the outputs are parameters specifying policy distributions. We consider a FSO fronthaul network with $N = 5$ RRHs, $M = 2$ ANs, one BBU and $L = 5$ orthogonal carriers. RRHs are distributed uniformly at random at locations in $[-5km, 5km]^2$ and ANs are distributed in $[-1km, 1km]$. System parameters are set as: $B = 10^9 Hz$, $T_f = 10^{-9} s$, $\epsilon = 1$, $P_t = 1.5W$, $P_s = 0.6W$, $R = 0.75A/W$ and $C_t = 50$.

Due to the data congestion constraints, the baseline policy becomes infeasible in this problem. In particular, each RRH randomly selects ANs for signal transmission and it is then intuitive that there exists times when all RRHs transmit to the same AN which violates the data congestion constraints. To show this more precisely in numerical simulations, we test the baseline policy and plot data congestion constraint values in Fig. 10. We see that the constraints are easily broken in its implementation such that it cannot be used here. In fact, due to the difficulty of problem, there is no intuitive heuristic policy for comparison.

We plot in Fig. 11 the performance achieved by the SDG algorithm and the PDDL algorithm. The SDG also exhibits the better performance in this case. The PDDL learns a policy that achieves the close performance to that obtained by using the SDG, which demonstrates its near-optimal learning ability. We further stress that the PDDL can be performed in a model-free manner, thereby no model information is required in its implementation, which is however necessary in the SDG algorithm. In Fig. 12 and Fig. 13, we plot all constraint values for both algorithms. Fig. 12b-12f and Fig. 13b-13f show the total power limitations are satisfied at all RRHs, i.e., the sum-power of carriers converges to zero with the increase of iteration at each RRH. Fig. 12a and Fig. 13a illustrate that the data congestion constraint is also satisfied at each AN in our

algorithms, which is however violated in the baseline policy as shown in Fig. 10. These verify the feasibility of policies learned by the SDG and the PDDL.

Overall, we observe superior performance of the SDG and the PDDL algorithms in a number of applications in FSO networks. Given the fact that the SDG solves the resource allocation problem exactly, it demonstrates the best performance in all applications. The PDDL follows closely with a near-perfect performance. More importantly, it learns the resource allocation policy with no need of system models and is computationally efficient even if the problem becomes extremely complicated. In addition, we observe that the learning process of the PDDL may take more iterations to converge compared to the SDG. This can be explained by the large number of DNN parameters that need to be optimized and the model-free nature of its learning process. While oftentimes, we perform the learning process offline before implementation, such that the learning rate does not play an important role here.

VI. CONCLUSIONS

In this paper, we consider the optimal resource allocation in free space optical networks. The problem takes the form of constrained stochastic optimization, that is typically challenging due to the non-convex nature, multiple constraints and lack of model information. Examples include power adaptation, relay selection and their joint allocation. We first propose the model-based Stochastic Dual Gradient algorithm, which solves the problem exactly by exploiting a null duality gap property. However, it heavily relies on system models that may not be available in practice. The model-free Primal-Dual Deep Learning algorithm is then developed to overcome these issues. In particular, it parameterizes the resource allocation policy with Deep Neural Networks and learns optimal parameters by updating primal and dual variables simultaneously. Policy gradient method is further applied to the primal update in order to estimate necessary gradient information without using the knowledge of system or channel models. Numerical experiments are performed in a number of applications to show superior performance of our algorithms. The model-free PDDL algorithm proposed in this paper has wide applications for problems in FSO networks and communications, where optical

systems are too sophisticated and atmospheric channels are too complicated to model.

REFERENCES

- [1] Z. Gao, M. Eisen, and A. Ribeiro, "Optimal wdm power allocation via deep learning for radio on free space optics systems," in *2019 IEEE Global Communications Conference (GLOBECOM)*. IEEE, 2019, pp. 1–6.
- [2] X. Zhu and J. M. Kahn, "Free-space optical communication through atmospheric turbulence channels," *IEEE Transactions on communications*, vol. 50, no. 8, pp. 1293–1300, 2002.
- [3] M. A. Khalighi and M. Uysal, "Survey on free space optical communication: A communication theory perspective," *IEEE communications surveys & tutorials*, vol. 16, no. 4, pp. 2231–2258, 2014.
- [4] V. W. S. Chan, "Free-space optical communications," *Journal of Lightwave technology*, vol. 24, no. 12, pp. 4750–4762, 2006.
- [5] R. Martini, C. Bethea, F. Capasso, C. Gmachl, R. Paiella, E. A. Whittaker, H. Y. Hwang, D. L. Sivco, J. N. Baillargeon, and A. Y. Cho, "Free-space optical transmission of multimedia satellite data streams using mid-infrared quantum cascade lasers," *Electronics Letters*, vol. 38, no. 4, pp. 181–183, 2002.
- [6] J. Akella, M. Yuksel, and S. Kalyanaraman, "Multi-channel communication in free-space optical networks for the last-mile," in *2007 15th IEEE Workshop on Local & Metropolitan Area Networks*. IEEE, 2007, pp. 43–48.
- [7] E. Leitgeb, J. Bregerzer, M. Gebhart, P. Fasser, and A. Merdonig, "Free-space optics: Broadband wireless supplement to fiber networks," in *Free-Space Laser Communication Technologies XV*, vol. 4975. International Society for Optics and Photonics, 2003, pp. 57–68.
- [8] M. Alzenad, M. Z. Shakir, H. Yanikomeroglu, and M. Alouini, "Fso-based vertical backhaul/fronthaul framework for 5g+ wireless networks," *IEEE Communications Magazine*, vol. 56, no. 1, pp. 218–224, 2018.
- [9] L. C. Andrews and R. L. Phillips, "Laser beam propagation through random media." SPIE, 2005.
- [10] D. K. Borah and D. G. Voelz, "Pointing error effects on free-space optical communication links in the presence of atmospheric turbulence," *Journal of Lightwave Technology*, vol. 27, no. 18, pp. 3965–3973, 2009.
- [11] Z. Gao, J. Zhang, and A. Dang, "Beam spread and wander of gaussian beam through anisotropic non-kolmogorov atmospheric turbulence for optical wireless communication," in *2017 IEEE International Conference on Communications Workshops (ICC Workshops)*. IEEE, 2017, pp. 343–348.
- [12] Z. Gao, Y. Luo, and A. Dang, "Beam wander effects on scintillation theory of gaussian beam through anisotropic non-kolmogorov atmospheric turbulence for optical wireless communication," in *2018 IEEE International Conference on Communications Workshops (ICC Workshops)*. IEEE, 2018, pp. 1–6.
- [13] Z. Gao, Z. Li, and A. Dang, "Beam quality factor and its effect on laser beam through anisotropic turbulence for owc," in *2019 15th International Conference on Telecommunications (ConTEL)*. IEEE, 2019, pp. 1–7.
- [14] J. Zhang, R. Li, Z. Gao, and A. Dang, "Ergodicity of phase fluctuations for free-space optical link in atmospheric turbulence," *IEEE Photonics Technology Letters*, vol. 31, no. 5, pp. 377–380, 2019.
- [15] K. Kiasaleh, "Performance of apd-based, ppm free-space optical communication systems in atmospheric turbulence," *IEEE transactions on communications*, vol. 53, no. 9, pp. 1455–1461, 2005.
- [16] S. M. Navidpour, M. Uysal, and M. Kavehrad, "Ber performance of free-space optical transmission with spatial diversity," *IEEE transactions on wireless communications*, vol. 6, no. 8, pp. 2813–2819, 2007.
- [17] M. A. Kashani, M. Safari, and M. Uysal, "Optimal relay placement and diversity analysis of relay-assisted free-space optical communication systems," *Journal of Optical Communications and Networking*, vol. 5, no. 1, pp. 37–47, 2013.
- [18] C. Abou-Rjeily and A. Slim, "Cooperative diversity for free-space optical communications: Transceiver design and performance analysis," *IEEE Transactions on Communications*, vol. 59, no. 3, pp. 658–663, 2010.
- [19] C. Abou-Rjeily and S. Haddad, "Cooperative fso systems: Performance analysis and optimal power allocation," *Journal of Lightwave Technology*, vol. 29, no. 7, pp. 1058–1065, 2011.
- [20] H. Zhou, S. Mao, and P. Agrawal, "Optical power allocation for adaptive transmissions in wavelength-division multiplexing free space optical networks," *Digital Communications and Networks*, vol. 1, no. 3, pp. 171–180, 2015.
- [21] H. Zhou, D. Hu, S. Mao, and P. Agrawal, "Joint relay selection and power allocation in cooperative fso networks," in *2013 IEEE Global Communications Conference (GLOBECOM)*. IEEE, 2013, pp. 2418–2423.
- [22] K. Park, Y. Ko, and M. Alouini, "On the power and offset allocation for rate adaptation of spatial multiplexing in optical wireless mimo channels," *IEEE Transactions on Communications*, vol. 61, no. 4, pp. 1535–1543, 2013.
- [23] M. Safari and M. Uysal, "Relay-assisted free-space optical communication," *IEEE Transactions on Wireless Communications*, vol. 7, no. 12, pp. 5441–5449, 2008.
- [24] M. Karimi and M. Nasiri-Kenari, "Free space optical communications via optical amplify-and-forward relaying," *Journal of Lightwave Technology*, vol. 29, no. 2, pp. 242–248, 2011.
- [25] —, "Ber analysis of cooperative systems in free-space optical networks," *Journal of Lightwave Technology*, vol. 27, no. 24, pp. 5639–5647, 2009.
- [26] N. D. Chatzidiamantis, D. S. Michalopoulos, E. E. Kriezis, G. K. Karagiannidis, and R. Schober, "Relay selection protocols for relay-assisted free-space optical systems," *IEEE/OSA Journal of Optical Communications and Networking*, vol. 5, no. 1, pp. 92–103, 2013.
- [27] C. Abou-Rjeily, "Performance analysis of selective relaying in cooperative free-space optical systems," *Journal of lightwave technology*, vol. 31, no. 18, pp. 2965–2973, 2013.
- [28] M. Z. Hassan, M. J. Hossain, J. Cheng, and V. C. Leung, "Statistical delay-qos aware joint power allocation and relaying link selection for free space optics based fronthaul networks," *IEEE Transactions on Communications*, vol. 66, no. 3, pp. 1124–1138, 2017.
- [29] M. Z. Hassan, V. C. Leung, M. J. Hossain, and J. Cheng, "Delay-qos aware adaptive resource allocations for free space optical fronthaul networks," in *2017 IEEE Global Communications Conference (GLOBECOM)*. IEEE, 2017, pp. 1–6.
- [30] W. Liu, Z. Wang, X. Liu, N. Zeng, Y. Liu, and F. E. Alsaadi, "A survey of deep neural network architectures and their applications," *Neurocomputing*, vol. 234, pp. 11–26, 2017.
- [31] A. Canziani, A. Paszke, and E. Culurciello, "An analysis of deep neural network models for practical applications," *arXiv preprint arXiv:1605.07678*, 2016.
- [32] C. Sánchez-Sánchez and D. Izzo, "Real-time optimal control via deep neural networks: study on landing problems," *Journal of Guidance, Control, and Dynamics*, vol. 41, no. 5, pp. 1122–1135, 2018.
- [33] H. Sun, X. Chen, Q. Shi, M. Hong, X. Fu, and N. D. Sidiropoulos, "Learning to optimize: Training deep neural networks for wireless resource management," in *2017 IEEE 18th International Workshop on Signal Processing Advances in Wireless Communications (SPAWC)*. IEEE, 2017, pp. 1–6.
- [34] Z. Xu, Y. Wang, J. Tang, J. Wang, and M. C. Gursoy, "A deep reinforcement learning based framework for power-efficient resource allocation in cloud rans," in *2017 IEEE International Conference on Communications (ICC)*. IEEE, 2017, pp. 1–6.
- [35] M. Eisen, C. Zhang, L. F. O. Chamon, D. D. Lee, and A. Ribeiro, "Learning optimal resource allocations in wireless systems," *IEEE Transactions on Signal Processing*, vol. 67, no. 10, pp. 2775–2790, 2019.
- [36] A. Ribeiro, "Optimal resource allocation in wireless communication and networking," *EURASIP Journal on Wireless Communications and Networking*, vol. 2012, no. 1, p. 272, 2012.
- [37] K. Kazaura, K. Wakamori, M. Matsumoto, T. Higashino, K. Tsukamoto, and S. Komaki, "Rofso: a universal platform for convergence of fiber and free-space optical communication networks," *IEEE Communications Magazine*, vol. 48, no. 2, pp. 130–137, 2010.
- [38] L. Bottou, "Stochastic gradient descent tricks," in *Neural networks: Tricks of the trade*. Springer, 2012, pp. 421–436.
- [39] J. Park and I. W. Sandberg, "Universal approximation using radial-basis-function networks," *Neural computation*, vol. 3, no. 2, pp. 246–257, 1991.
- [40] B. Sriperumbudur, K. Fukumizu, and G. Lanckriet, "On the relation between universality, characteristic kernels and rkhs embedding of measures," in *Proceedings of the thirteenth international conference on artificial intelligence and statistics*, 2010, pp. 773–780.
- [41] K. Hornik, M. Stinchcombe, and H. White, "Multilayer feedforward networks are universal approximators," *Neural networks*, vol. 2, no. 5, pp. 359–366, 1989.
- [42] R. S. Sutton, D. A. McAllester, S. P. Singh, and Y. Mansour, "Policy gradient methods for reinforcement learning with function approximation," in *Advances in neural information processing systems*, 2000, pp. 1057–1063.